The Journal of Chemical Physics

First principles theoretical spectroscopy of methylene blue: Between limitations of time-dependent density functional theory approximations and its realistic description in the solvent

Cite as: J. Chem. Phys. **154**, 044106 (2021); https://doi.org/10.1063/5.0029727
Submitted: 15 September 2020 . Accepted: 01 January 2021 . Published Online: 26 January 2021

Thiago B. de Queiroz, Erick R. de Figueroa, Maurício D. Coutinho-Neto, Cleiton D. Maciel, Enrico Tapavicza, Zohreh Hashemi, and Linn Leppert

The Journal of Chemical Physics ARTICLE scitation.org/journal/jcp

First principles theoretical spectroscopy of methylene blue: Between limitations of time-dependent density functional theory approximations and its realistic description in the solvent

Cite as: J. Chem. Phys. 154, 044106 (2021); doi: 10.1063/5.0029727
Submitted: 15 September 2020 • Accepted: 1 January 2021 •
Published Online: 26 January 2021

Thiago B. de Queiroz,[1,a] Erick R. de Figueroa,[1] Maurício D. Coutinho-Neto,[1,b] Cleiton D. Maciel,[2] Enrico Tapavicza,[3,a] Zohreh Hashemi,[4] and Linn Leppert[4,5,c]

AFFILIATIONS

[1]Centro de Ciências Naturais e Humanas, Universidade Federal do ABC, Av. dos Estados 5001, 09510-580 Santo André-SP, Brazil
[2]Instituto Federal de Educação, Ciência e Tecnologia de São Paulo, Campus Itaquaquecetuba, Avenida Primeiro de Maio, 500, 08571-050 Itaquaquecetuba-SP, Brazil
[3]Department of Chemistry and Biochemistry, California State University, Long Beach, 1250 Bellflower Boulevard, Long Beach, California 90840, USA
[4]Institute of Physics, University of Bayreuth, Bayreuth 95440, Germany
[5]MESA+ Institute for Nanotechnology, University of Twente, 7500 AE Enschede, The Netherlands

[a]**Authors to whom correspondence should be addressed:** thiago.branquinho@ufabc.edu.br and enrico.tapavicza@csulb.edu
[b]mauricio.neto@ufabc.edu.br
[c]l.leppert@utwente.nl

ABSTRACT

Methylene blue [3,7-Bis(di-methylamino) phenothiazin-5-ium chloride] is a phenothiazine dye with applications as a sensitizer for photodynamic therapy, photoantimicrobials, and dye-sensitized solar cells. Time-dependent density functional theory (TDDFT), based on (semi)local and global hybrid exchange-correlation functionals, fails to correctly describe its spectral features due to known limitations for describing optical excitations of π-conjugated systems. Here, we use TDDFT with a non-empirical optimally tuned range-separated hybrid functional to explore the optical excitations of gas phase and solvated methylene blue. We compute solvated configurations using molecular dynamics and an iterative procedure to account for explicit solute polarization. We rationalize and validate that by extrapolating the optimized range separation parameter to an infinite amount of solvating molecules, the optical gap of methylene blue is well described. Moreover, this method allows us to resolve contributions from solvent–solute intermolecular interactions and dielectric screening. We validate our results by comparing them to first-principles calculations based on the GW+Bethe–Salpeter equation approach and experiment. Vibronic calculations using TDDFT and the generating function method account for the spectra's subbands and bring the computed transition energies to within 0.15 eV of the experimental data. This methodology is expected to perform equivalently well for describing solvated spectra of π-conjugated systems.

I. INTRODUCTION

Phenothiazine dyes, such as methylene blue [MB, 3,7-Bis (di-methylamino) phenothiazin-5-ium chloride], are a technologically important class of π-conjugated heterocyclic molecules. They cover an extensive range of light assisted applications as sensitizers for photodynamic therapy,[1,2] photoantimicrobials,[3] and dye-sensitized solar cells.[4] These applications involve light absorption and

electronic transitions in the molecule, which are strongly influenced by surrounding molecules and the medium in which these molecules are solvated.[2,5] It is therefore important to describe the electronic structure and dynamics of this class of molecules in realistic environments accurately.[2]

Density functional theory (DFT) and time-dependent DFT (TDDFT) have been extensively employed for such studies since they are, in principle, exact theories while computationally efficient.[6–13] Low-lying valence states of organic compounds of intermediate size are usually well described by exchange-correlation (xc) functionals within the local density approximation (LDA)[7] and generalized gradient approximation (GGA, also called semilocal approximation)[14] as well as by their linear combination with non-local Fock-like exact exchange (EXX), the global hybrids[15,16] (see, for instance, Ref. 17). However, these "standard TDDFT approximations," i.e., LDA, GGA, and global hybrid xc-functionals, yield significant deviations for π–$\pi*$ valence transitions of some sets of π-conjugated systems in comparison to experimental and theoretical reference data,[18–24] which is a statement that is also valid for MB[25] and other related compounds.[26,27] The failure of standard TDDFT for intermediate or large π-conjugated systems has been the subject of an extensive number of studies.[18,21–23,28,29]

From the perspective of molecular topology, open chain π-conjugated systems can be categorized as either polyenes or polymethines.[18] Polyenes demonstrate π-density alternation in the bonds, but the structure is based on their σ-skeleton (alternating double and single bonds).[18,29] Polymethines, just as cyanine dyes, show similar alternating π-bonds but with the highest alternating density in the atomic positions.[18,29] MB can be regarded as a carbocyanine related compound. Additionally, MB is expected to present even higher electron delocalization of the π-electrons in the ground state, in comparison to other phenothiazine dyes, due to the presence of two strongly electron-donating dimethyl-amino groups located diametrically alongside the molecule.[5]

For polymethines, the lowest allowed excitation is composed of a single electronic configuration, well characterized by a single-particle HOMO–LUMO transition.[18,30] Yet, standard TDDFT substantially overestimates the transition energies.[18,31,32] These systems exhibit excited state charge densities that differ significantly from the ground state densities.[18,29] This error was later recast in terms of the very small magnitude of the exchange-correlation response kernel integrals.[33,34] This is a feature that is badly described by linear response TDDFT since the xc kernel is calculated as the functional derivative of the xc potential at the ground state density (in principle, an exact linear response formulation if time propagated, but time-independent in the adiabatic approximation).[35,36] Similarly to the polyene case, pure GGAs perform slightly better than their corresponding hybrids.[33]

Besides the errors caused by the approximations described above (as compared to reference calculation methods), there are also errors arising from the incorrect and unrealistic description of the medium (as compared to experimental data).[25] In fact, electron-hole interactions can be significantly weakened by the effect of dielectric screening on the Coulomb potential.[37] For instance, the correct prediction of the S_0–S_1 transition energy in azobenzene derivatives in comparison to experimental data from calculations with the GW and Bethe–Salpeter equation (GW + BSE) requires the consideration of solvent polarization effects (dielectric screening).[38] Intermolecular interactions also play a role. From the infrared absorption spectrum of MB in the gas phase in comparison to its hydrated crystalline state,[39] it was proposed that the functional group aside $N^+(CH_3)_2$ is H-bonding to a water molecule. Again, standard TDDFT approximations are ill-equipped for describing such effects since they can produce electron density delocalization errors and overestimate intermolecular interactions.[33,40] Finally, these approximations are not designed to appropriately describe the long-range dielectric screening,[41–43] scaling incorrectly at long distances [decaying faster than $-(1/R)$, where R is the electron–hole distance].[44–46]

More recently, (semi)local approximations have been combined with EXX using the error function [$\mathrm{erf}(\omega r)$] in the Coulomb operator. In these range-separated hybrid (RSH) functionals, a range separation parameter, ω, scales short- and long-range exchange terms such that (semi)local terms dominate at short range and EXX at long range [in this particular format, referred as the long-range corrected (LRC) functional].[47–49] This tempered mix of (semi)local and EXX takes advantage of the good performance of predominantly (semi)local hybrid functionals for describing valence transitions[15] while ensuring the correct asymptotic of the potential $(-1/R)$, thereby improving preceding approximations in many respects.[47–51] The range separation parameter can be empirically optimized[47,52,53] or tuned from first principles, by choosing ω such that the eigenvalue of the Kohn–Sham frontier orbital located in the solute approaches the ionization energy.[54,55] The optimally tuned (OT) RSH functionals have been used with great success for the prediction of charge-transfer excitations for a variety of complex molecular systems,[56–58] intermolecular interactions,[59] and dielectric screening.[55,59] In fact, the introduction of the non-local EXX term at long range in the RSH seems to be appropriate for introducing the correct field-counteracting behavior due to the environment. For instance, polarizabilities and second hyperpolarizabilities are correctly predicted using this approach.[60]

In this article, we report first principles OT-RSH TDDFT calculations for the low-lying excited states of MB in vacuum and water, aiming to describe the system realistically while gaining insight into the limitations of state-of-the-art TDDFT. We employed the RSH functional ωPBE (PBE exchange at short range)[49] optimally tuned for MB optimized in vacuum and solvated by water molecules. We circumvent problems associated with RSH tuning for solvated molecules by analyzing the orbital localization involved in the functional tuning. Furthermore, we rationalize and demonstrate that the spectroscopic features of MB represented in its aqueous medium are well characterized by the OT-RSH functional. We show that this is a consequence of the increased short-to-long GGA/EXX interchange distance in solution (ω^{-1}), leading to higher weights of semilocal GGA exchange in the description of the MB molecule while treating the solvent by a balanced mix of semilocal and EXX at long range. Furthermore, we show that the zero-point vibrational energy shifts the spectrum to lower energies relative to vertical transitions and that vibronic contributions are responsible for a shoulder at higher energy (in comparison to the maximum absorption). As reference data, we use a partially self-consistent GW + BSE approach with the optimally tuned ωPBE as the starting point (as benchmarked in Refs. 61 and 62) in addition to experimental data. Thus, we present an inexpensive TDDFT methodology to describe accurately the absorption spectrum of this important organic dye in an aqueous solution, which can be extended to describe

excited states of other π-conjugated systems in a complex chemical environment.

II. METHODS

The details of the generation of the molecular configurations, molecular dynamics, calculation of vibrational spectrum, and calculation of excited states with TDDFT and GW + BSE and the data obtained are listed in the supplementary material. We also discuss our strategy for optimally tuning the RSH in explicit solvated systems, basis set convergence, and starting point issues in the GW + BSE calculations in the supplementary material.

The geometries and vibronic spectrum were obtained from DFT/B3LYP/def2-SV(P) calculations (theory/xc-approximation/basis set) followed by molecular dynamics simulations [isothermal–isobaric (NPT) ensemble with T = 298 K and P = 1 atm]. The ground and excited state vibrational spectra were computed using analytical and numerical second derivatives.[63,64] The structures for excited state calculations were obtained from MD frames and labeled according to their MD step after reaching thermal equilibrium and the number of solvating water molecules (in parenthesis), namely, MB-01(20), MB-13(20), MB-19(13), MB-27(20), MB-31(23), MB-38(26), and MB-46(21). These structures were generated with a solvation cutoff of 3.2 Å, where solvation cutoff is the maximum distance between an MB atom and an atom in the water molecule selected for the calculations. The structure MB-31 was taken as a representative structure and progressively solvated with additional cutoffs of 3.8 Å, 4.0 Å, 4.2 Å, 4.4 Å, 4.5 Å, 4.6 Å, 4.8 Å, 5.0 Å, 5.2 Å, and 5.4 Å, corresponding to 46, 58, 59, 67, 70, 71, 76, 84, 93, and 101 water molecules, respectively. The excited states were calculated from (i) TDDFT calculations with the functionals $xPBE_x + (1 - x)$ EXX + PBE_c, $0 \le x \le 1$, with the 6-31G(d,p) as basis set, (ii) TDDFT with the ωPBE and 6-31G(d,p) as functional and basis set, and (iii) eigenvalue self-consistent G_nW_n + BSE/ωPBE/6-311++(2d,2p) (method/starting point/basis set).

III. RESULTS

A. Ground state properties

MB and solvent configurations were obtained using an iterative procedure to account for solute polarization described in detail in the supplementary material. We employ a protocol to induce the solvent perturbation on the solute by generating an average solvent electrostatic potential (ASEP) developed initially by Sánchez and co-workers.[65,66] We follow a sequential QM/MM iterative procedure similar to the one proposed by Coutinho *et al.*[67,68] to generate converged solvent configurations in equilibrium with induced solute polarization for fixed solute geometries. In their procedure, solvent effects are included using point changes whose configurations come from Metropolis Monte Carlo simulations while solute charges are computed using the CHELPG algorithm.[69] An iterative procedure is used, where at each iteration a new set of solute CHELPG charges is obtained at distinct sampled solvent configurations. They have applied their method for the calculation of condensed phase spectra of several systems with encouraging results.[70–72]

Solvated MB displays a strong increase in dipole moment in the water when compared to vacuum, going from 2.55 D to 4.23 D as computed by our iterative procedure. A strong charge separation matches the increase of the dipole moment of the molecule, where the central nitrogen acquires a strongly negative charge compared to its vacuum value. CHELPG values increase from $-0.60e$ to $-0.91e$. As expected, solute–solvent interactions are affected, resulting in a larger number of hydrogen bonds between the central nitrogen and water. These interactions are present in most configurations sampled from molecular dynamics and in the configurations selected for spectroscopic studies.

B. Excited states of the isolated MB by exploring global hybrid functionals: Assignment of the failures and the OT-RSH proposal

As we expect that standard TDDFT cannot describe the optical gap of MB well, we try to map possible error sources by calculating the first excited state transitions (S_0–S_1 and S_0–T_1), adding EXX stepwise in the hybrid functional. Figure 1 shows the S_1 and T_1 excitation energies calculated with TDDFT as a function of EXX/PBE_x admixture for MB-31(0), as well as calculated from the G_nW_n + BSE method [$\Delta E(S_0–S_1)$ = 2.25 eV and $\Delta E(S_0–T_1)$ = 1.00 eV] and the experimental maximum absorption of MB in water (1.87 eV).[73] The experimental value taken in water does not represent the optical gap of the molecule in the gas phase, but solvent effects are not expected to exceed 0.1 eV–0.4 eV (see below). Thus, the optical gap of the molecule in the gas phase should be around 2.0 eV–2.3 eV, suggesting that G_nW_n + BSE can be regarded as the reference data (also rationalized in Refs. 61 and 62). The S_0–S_1 transition energy approaches the G_nW_n + BSE and the experimental values as the

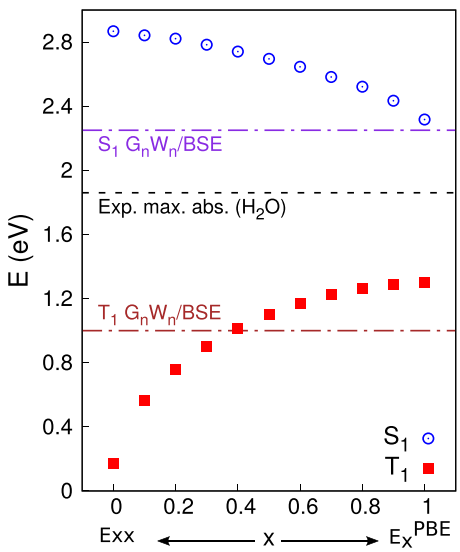

FIG. 1. S_0–S_1 and S_0–T_1 transition energies for MB-31(0) as a function of PBE exchange and exact Fock exchange admixture in the TDDFT approximation [E_x = $xPBE_x$ + (1-x)EXX] and in comparison to G_nW_n + BSE calculations and the experimental maximum absorption of MB in water.

GGA portion increases, going from 2.87 eV when E_x = EXX to 2.32 eV when E_x = PBE$_x$. Simultaneously, S_0–T_1 increases from the unrealistic value of ≈0.1 eV when E_x = EXX to the reasonable value of ≈1.2 eV when E_x = PBE$_x$. Yet, either TDDFT or GW + BSE estimates for the S_0–T_1 transition are considerably underestimated, in comparison with reference data (1.75 eV using CASPT2),[74] due to triplet instabilities.[75–78]

The superior performance of pure GGAs over HF indicates that charge transfer is not a dominant feature and that the transition could be of double excitation character (when error cancellations occur for GGAs).[23] However, the overestimation of the optical gap resembles the case of the cyanine dyes,[18,33,34] when the dynamical correlation is important, as well as the fact that the pure GGAs outperform their associated hybrids.[33] We could calibrate the global hybrid functional with high portions of GGA and proceed further to study the influence of the solvent in the optical gap of MB. However, besides the lack of generality of such procedure, from previous studies, we learn that the optimally tuned RSH can describe well intermolecular interactions[59,79] and dielectric screening,[55] differently from global hybrids.[59] Furthermore, short-contact intermolecular interactions with solvent molecules could lead to an increase in the charge-transfer character of the first excited state, another feature that is well described by RSH functionals in contrast to hybrid functionals,[79] especially if constructed with large portions of GGA.

Figure 2 shows the electron–hole pair of the natural transition orbitals (NTOs) of MB-31(0) for the S_0–S_1 transition from TDDFT/ωPBE calculations. The transition is almost entirely represented by a HOMO–LUMO transition (> 90%) and described by the electron migration from the whole molecule to the central sulfur and nitrogen atoms, an apparent valence excitation with little intramolecular charge transfer character. The TDDFT/ωPBE calculations estimate the S_0–S_1 and S_0–T_1 transitions at 2.54 eV and 1.22 eV, respectively. These transitions are off by ≈0.3 eV in comparison with G_nW_n + BSE, slightly worse than the pure PBE and desired accuracy (within ≈0.1 eV).

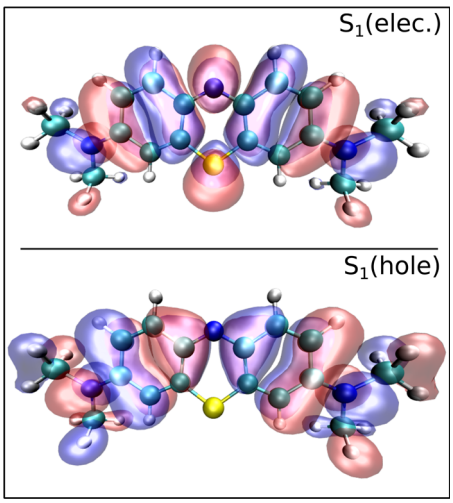

FIG. 2. NTO isosurface densities of the most significant electron–hole pair (⩾ 90%) of S_1 for MB-31(0). Carbon atoms are represented in green, nitrogen in blue, sulfur in yellow, and hydrogen in white.

We anticipate that the inferior performance of the OT-RSH with respect to the GGA will be attenuated or removed when inserting solvent effects. The optimal ω for the solvated structures tends to be smaller since the frontier orbitals tend to be more delocalized.[43] Thus, the distance where the fraction of EXX is larger than the PBE exchange increases, such that a larger contribution to the energy of MB comes from the GGA exchange potential.[43] For instance, according to the optimal ω values, the GGA/EXX interchange distance for the isolated molecule is at 1.3 Å and for the fully solvated system at 1.7 Å [taken from erf($\omega_{opt} r_0$) = 1/2, see ω optimization below]. Furthermore, the OT-RSH is indicated for explicitly solvated systems because GGAs tend to overestimate electron density delocalization while EXX tends to underestimate it, such that the OT-RSH temper these limits showing small delocalization errors.[33]

C. Excited states from TDDFT/ωPBE and the contributions from intermolecular interactions and dielectric screening

Table I lists the TDDFT/ωPBE transition energies of the first excited states with respective oscillator strengths for singlets of all configurations (note that triplet transitions are forbidden in our calculations due to the lack of spin–orbit coupling). Figure 3 illustrates the transitions in comparison with the experimental data. The excited states with strong oscillator strength (~0.5) are always localized in MB, topologically similar to the transition of the isolated molecule, as noted by their electron–hole pair from the NTOs [see representative NTOs in Fig. 4-left for MB-31(101)]. The singlet transitions with low oscillator strength are of a mixed charge transfer character, described by the electron donation from a water molecule nearby the sulfur atom of MB [represented in Fig. 4-right for MB-31(101)]. For most of the configurations, this excitation is about 0.1 eV–0.4 eV distant from the excitation localized in MB, and its oscillator strength is limited to 10^{-2}. Interestingly, for the configuration MB-31(23), this excitation is the lowest one and shows increased oscillator strength, 0.07, and it is much closer, in energy, to the one located in MB (ΔE = 0.036 eV). This indicates that there might be a coupling between S_1 and S_2, such that S_1 increases in oscillator strength, pulling the absorption band to lower energies (similar to the coupling reported in Ref. 80). Note that by taking into consideration the structures generated with a solvent cutoff of 3.2 Å with 20–21 solvent molecules, the dispersion in the optical gap is about 0.3 eV, which is related to small molecular distortions and distinct solvent configurations (similarly to the configurational variances when collecting the experimental data, but here limited to a small number of sampling configurations).

After looking at the optical gap dispersion of MB due to distinct molecular arrangements and a variation of intermolecular interactions, we look at MB-31 as a representative configuration to investigate the influence of intermolecular interaction and dielectric screening in the first excited states. Thus, structures with various distance cutoffs with respect to solvent molecules were generated and the optimization parameter was calculated as a function of the

TABLE I. First excited states and oscillator strengths (O.S.) for MB structures as calculated by the TDDFT/ωPBE method. Note that ω_{EA} is used for all calculations except for MB-31(101), in which ω_{solv}^{ext} was used instead, which is the optimal ω extrapolated to a completely solvated system.

Molecule	ω_{opt} ($\times 10^{-3}$ a_0^{-1})	S_1 (eV)	O.S.$_{S_1}$	S_2 (eV)	O.S.$_{S_2}$	T_1 (eV)	T_2 (eV)
MB-01(20)	182	1.6316	0.0008	2.3508	0.4767	1.0563	1.6293
MB-13(20)	182	2.3099	0.7991	2.4412	0.0181	0.9131	1.6807
MB-19(13)	191	2.3813	0.8285	2.5467	0.0014	0.9977	1.8134
MB-27(20)	182	2.5791	0.8002	2.6941	0.0056	1.2580	1.9027
MB-38(26)	179	2.2398	0.6958	2.3912	0.0009	0.8197	1.6489
MB-46(21)	179	1.9670	0.0055	2.3705	0.7052	1.0959	1.6642
MB-31(0)	203	2.5432	0.8694	2.7871	0.0063	1.2233	1.9838
MB-31(23)	179	2.1800	0.0701	2.2160	0.6484	0.7460	1.7490
MB-31(101)	150	2.1527	0.7135	2.3240	0.0079	0.8199	1.6509

number of solvent molecules. The optimization parameter could be represented by a mono-exponential decay as the number of solvent molecules (n) increases, described as $\omega(n) = \omega_0 \exp(-n/\delta) + \omega_{solv}^{ext}$, where ω_0 is the optimal ω of the bare structure, δ is a system dependent fitting parameter, and ω_{solv}^{ext} is the optimal ω when extrapolating the optimization to the fully solvated structure ("bulk" water).[55] Interestingly, the exponential decay of the parameter ω as a function of the solvation shell number is not only observed for weakly intermolecular interacting systems, as demonstrated in Ref. 55 but also for a system of polar molecules prone to intermolecular interaction.

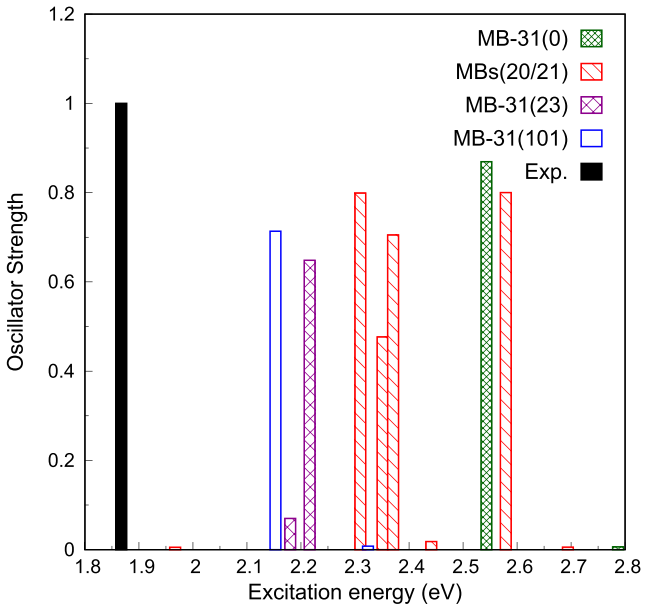

FIG. 3. Excited state spectra for MB-31(0), in green; MB-01(20), MB-13(20), MB-27(20), and MB-46(21), in red; MB-31(23), in magenta; and MB-31(101), in blue, as calculated by the TDDFT/ωPBE method, and experimental data, in black.

Using ω_{solv}^{ext} in TDDFT/ωPBE calculations, one can account for the long-range dielectric screening of the media in the description of the excited states.[55,81] Figure 5 shows a good agreement between the approximate curve and the ΔSCF-calculated $\omega(n)$, which resulted in an ω_{solv}^{ext} value of 0.150 a_0^{-1}.

The comparison between the optical gap of MB as calculated from the G_nW_n + BSE and TDDFT/ωPBE methodologies is illustrated in Fig. 6. The S_0–S_1 transition of MB-31(23) from the G_nW_n + BSE calculation is at 2.05 eV, indicating a decrease in 0.2 eV due to intermolecular interactions and local screening. TDDFT/ωPBE predicts the S_0–S_1 transition of MB-31(23) at 0.36 eV below the transition for the isolated molecule. The OT-RSH is more influenced by the explicit solvation because the range separating parameter decays rapidly by including the first coordination shell, and the lowering of the parameter emulates long-range dielectric screening.[55] For instance, ω decays from 0.203 to 0.179 a_0^1 by including the first coordination shell (88% of ω_0), reaching 0.150 a_0^1 when the parameter is extrapolated to fully solvated structure (74% of ω_0).

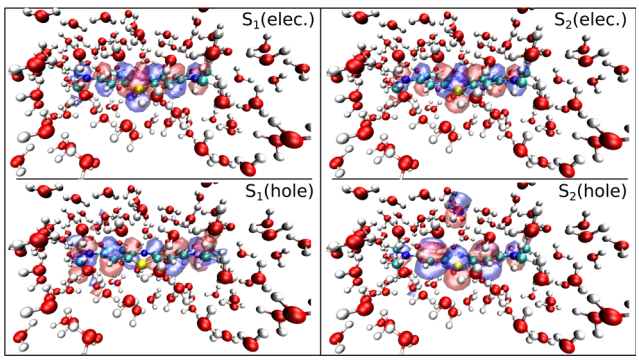

FIG. 4. NTO isosurface densities of the most significant electron–hole pair (⩾90%) of the S_1 and S_2 transitions for MB-31(101) as calculated by the TDDFT/ωPBE method. Carbon atoms are represented in green, nitrogen in blue, sulfur in yellow, oxygen in red, and hydrogen in white.

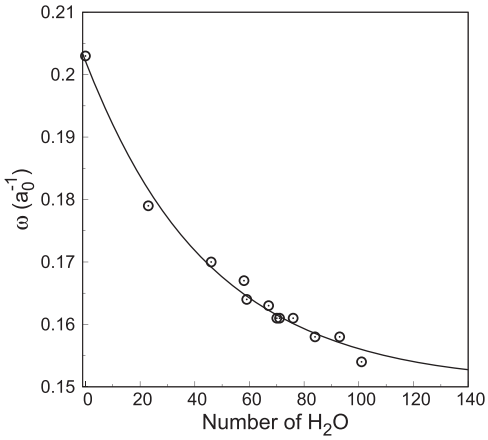

FIG. 5. Optimal ω as a function of the number of water solvent molecules surrounding MB-31 and exponential decay fits.

Moving to the fully solvated structure, one notes an additional shift to the lower energy of about 0.03 eV, with all results indicating a modest contribution from long-range dielectric screening in the first excited singlet state. This is expected since MB is considered a dye with a small solvatochromic shift.[5,82] Note that the calculation of MB-31(101) results in a S_0–S_1 with a deviation of 0.28 eV to higher energies in comparison to experimental data. Vibronic and zero point corrections shift this value further down, as described in Sec. III D.

The performance of TDDFT for cyanine dyes has been previously analyzed as follows:[33] An electronic transition with a strong HOMO–LUMO character in the adiabatic approximation is approximately given by the HOMO–LUMO gap ($\varepsilon_L - \varepsilon_H$), added by the Coulomb electron–electron repulsion term and xc kernel integrals.[33] For instance, for the two-level model HOMO–LUMO transition in the Tamm–Dancoff approximation,[33]

$$E_{S1}^{TDDFT} = (\varepsilon_L - \varepsilon_H) + 2[LH|r_{12}^{-1}|LH] + [LH|f_{xc}^{\alpha\alpha} + f_{xc}^{\alpha\beta}|LH], \quad (1)$$

where the second term on the right-hand side of the equation is a two-electron repulsion integral and the third term is the xc linear response kernel (f_{xc}) integral (L and H refer to the HOMO and LUMO Kohn–Sham orbitals, respectively, and α and β are spin labels). The HOMO–LUMO gap is the dominant positive term, the electron–electron Coulomb repulsion term is typically small but positive, and the xc kernel integrals are generally negative.

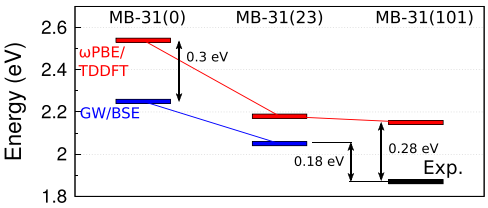

FIG. 6. Diagram of the first excited state for MB-31(0) and MB-31(23) as calculated from the G_nW_n + BSE and TDDFT/ωPBE methods, in addition to the TDDFT/ωPBE calculation for MB-31(101), and experimental data.

The HOMO–LUMO gap for MB-31(0) as calculated from DFT/ωPBE is 4.5 eV (similar to the other configurations). Thus, the last term of the above equation, the xc kernel integrals, should be sufficiently large (and negative) in order to lower the optical gap in the direction of the reference data (E_{S1}^{GW+BSE} = 2.25 eV). The fact that the TDDFT/ωPBE results are generally overestimating those of the G_nW_n + BSE is similar to what has been observed for cyanine dyes, and has been attributed to too small contributions of the xc response kernel integrals.[33,34]

D. Vibronic contributions

Another question regarding the absorption spectrum of MB is related to the shape of the envelope, in particular the cause of the line broadening and the shoulder between 625 nm and 606 nm (1.98 eV and 2.04 eV, or 16 000 cm^{-1} and 16 500 cm^{-1}, respectively) (Fig. 7). Within the generating function method,[83,84] the 0–0 transition occurs at

$$\Delta E_{0-0} = \Delta E_{adia} - E_{ZPV}^{0} + E_{ZPV}^{1}, \quad (2)$$

where ΔE_{adia} is the adiabatic excitation energy, and the last two terms are the zero-point vibrational energy (ZPV) in the ground

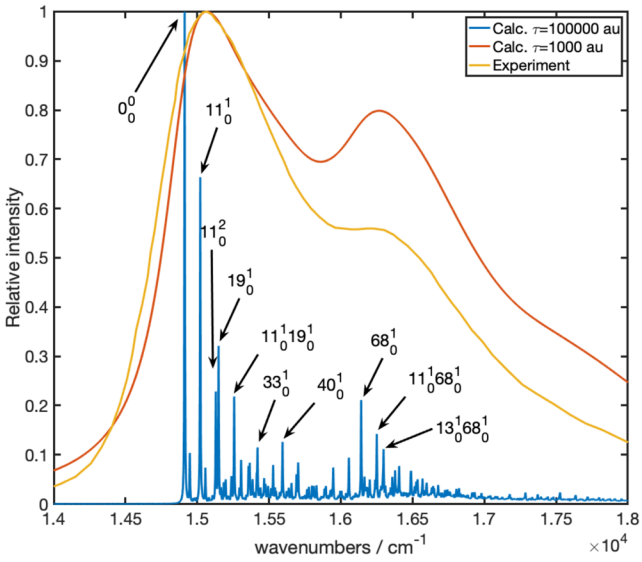

FIG. 7. Comparison between the calculated vibronic absorption spectrum in the gas phase and the experimentally measured spectrum in water.[73] Computed spectra have been downshifted by 0.5 eV (4046 cm^{-1}) to align the main band of the broad spectrum with the experimental λ_{max} value. 0_0^0 denotes the 0–0 transition. In the other peak assignments, the mode number according to Table S2 (supplementary material) is given with subscripts indicating its ground state vibrational quantum number and superscripts indicating its excited state vibrational quantum number of the transition; all other modes have both zero as initial and final quantum numbers.

and excited states, respectively. The 0–0 transition (denoted 0_0^0 in Fig. 7) serves as the reference point for the vibronic structure. Since the excited state ZPV energy (8.458 eV) is smaller than the ground state ZVP (8.532 eV), the 0–0 transition (2.351 eV) lies 0.16 eV below the TDDFT/B3LYP/def2-SVP adiabatic excitation energy of 2.424 eV. When applying a line broadening with a lifetime of 1000 au (red in Fig. 7), the peak maximum is shifted 0.019 eV to the blue, relative to the 0–0 transition using a lifetime of 100 000 au (blue in Fig. 7). In general, line broadening could be caused by conformational isomers[85,86] or by vibronic bands.[83] Our vibronic spectra calculations, including Duschinsky effects, show that both line broadening and the dominant shoulder are due to the vibronic effects. Furthermore, the line broadening is mainly caused by three vibrational modes, mode 11, mode 19, and mode 40, shown in Fig. 8 (Multimedia view)—(Table S2 lists all vibrational transitions in the supplementary material). By assigning modes 11 and 19 as the main causes for the broadening, our calculations are partially consistent with previous calculations of Franck–Condon factors by Dean and co-workers based on the displaced harmonic oscillator model; however, mode 40 was not identified by their work.[73] In addition, several peaks with minor intensity (<0.1 in Fig. 7) contribute to broadening and were not included in previous spectral simulations.[73] Regarding the dominant shoulder above 625 nm (16 000 cm^{-1}), our calculations show that it is mainly due to mode 68 and its combinations with modes 11 and 13 (Fig. 7).

We also computed the vibronic spectrum using the ωPBE xc-functional [6-31G(d,p) basis set and $\omega = 0.203 a_0^{-1}$] but within the displaced harmonic oscillator approximation because we could not determine the full Duschinsky matrix from the output. However, since the Duschinsky matrix for MB is close to unity, the approximation made is small. The ωPBE vibronic spectrum compares well to the TD-B3LYP spectrum (see the supplementary material).

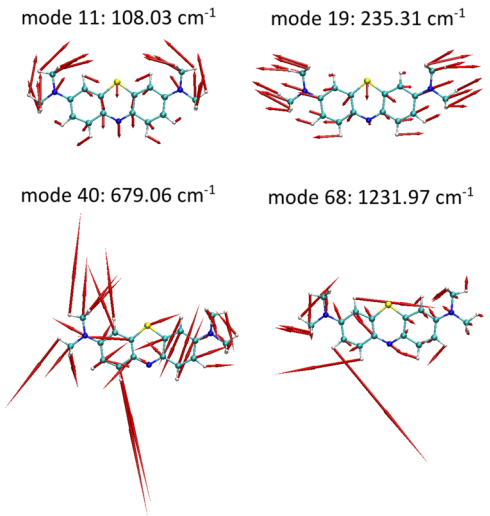

FIG. 8. Dominant excited state vibrational normal modes and their frequencies calculated by TDDFT/B3LYP/def2-SVP. Multimedia views: https://doi.org/10.1063/5.0029727.1; https://doi.org/10.1063/5.0029727.2; https://doi.org/10.1063/5.0029727.3; https://doi.org/10.1063/5.0029727.4

As expected, the vibrational features are relatively insensitive to the xc-functional approximation. In addition, we computed the TD-B3LYP/TDA vibronic spectrum. Vibrational frequencies in the excited state are very similar in TD-B3LYP and TD-B3LYP/TDA, but some peak intensities are different in the two spectra due to differences in the Duschinsky matrix (see the supplementary material). This shows that the TDA affects the computation of the vibrational modes in the excited state.

IV. CONCLUSIONS

We present a strategy to predict the optical gap of MB in water using an optimally tuned range-separated hybrid functional for fully solvated structures within TDDFT. The addition of a realistic solvent environment, dielectric screening effects, and vibronic corrections are essential for bringing the results close to experiments. Solvation effects, which we take into account explicitly, are responsible for lowering the optical gap by about 0.2 eV–0.4 eV, resulting in an overestimation of the experimental data by 0.2 eV–0.3 eV depending on the structure used. Vibronic effects and zero-point corrections shift the adiabatic value down in energy by 0.16 eV, as estimated by TDDFT/B3LYP calculations. The overestimation then decreases to only ~0.15 eV with respect to experimental data. Vibronic calculations also show that in-plane mode 68, with a large component in ring CH bending, and mode 11 are responsible for the vibronic subband that is very characteristic of MB's UV spectra in solution.

The optical gap difference between G_nW_n + BSE and TDDFT/ωPBE is reduced from 0.3 eV to 0.1 eV by going from the isolated MB to the solvated structure. The improvement in the performance of TDDFT/ωPBE for the solvated structure occurs because the semilocal term of the functional takes over at larger distances, and dielectric screening is emulated by choosing the range separation parameter appropriately.[55] Since semilocal functionals are reported to treat better π-conjugated systems (although due to error cancellations),[20,23,33] we expect that such a strategy might be generalized, permitting to study these important systems at relatively low computational cost and with acceptable accuracy. The combination of the methodologies employed in this study is going to be relevant for the description of the absorption spectra of π-conjugated systems, especially in solution or in other chemical environments.

SUPPLEMENTARY MATERIAL

See the supplementary material for details about molecular configurations, vibronic spectra calculations and illustrative movies of the relevant vibrational modes, optimal tuning of the RSH functional and TDDFT calculations, GW + BSE calculations: starting point dependence and basis set convergence, and tables with data obtained in the optimal tuning of the RSH functional and GW + BSE calculations, and the vibronic modes.

ACKNOWLEDGMENTS

T.B.d.Q. acknowledges the support of CNPq (Universal Grant No. 404951/2016-3). Z.H. and L.L. acknowledge the support of the

Bavarian State Ministry of Science and the Arts through the Collaborative Research Network Solar Technologies go Hybrid (SolTech), the Elite Network Bavaria (ENB), and computational resources provided by the Bavarian Polymer Institute (BPI). M.D.C.-N. acknowledges the support of FAPESP (Grant No. 12/50680-5). This study was financed, in part, by the Coordenação de Aperfeiçoamento de Pessoal de Nível Superior–Brasil (CAPES), Finance Code 001. The authors are thankful to the University of Bayreuth-Theoretical Physics IV for computational time and Professor Stephan Kümmel for valuable discussions.

DATA AVAILABILITY

The data that support the findings of this study are available from the corresponding author upon reasonable request.

REFERENCES

[1] A. Ormond and H. Freeman, Materials **6**, 817 (2013).
[2] J. C. Dean, D. G. Oblinsky, S. Rafiq, and G. D. Scholes, J. Phys. Chem. B **120**, 440 (2016).
[3] M. Wainwright, J. Braz. Chem. Soc. **26**, 2390 (2015).
[4] Z.-S. Huang, H. Meier, and D. Cao, J. Mater. Chem. C **4**, 2404 (2016).
[5] C. Párkányi, C. Boniface, J. J. Aaron, and M. Maafi, Spectrochim. Acta A **49**, 1715 (1993).
[6] P. Hohenberg and W. Kohn, Phys. Rev. **136**, B864 (1964).
[7] W. Kohn and L. J. Sham, Phys. Rev. **140**, A1133 (1965).
[8] E. Runge and E. K. U. Gross, Phys. Rev. Lett. **52**, 997 (1984).
[9] D. Rappoport and F. Furche, J. Am. Chem. Soc. **126**, 1277 (2004).
[10] K. Burke, J. Werschnik, and E. K. U. Gross, J. Chem. Phys. **123**, 062206 (2005).
[11] J. Schirmer and A. Dreuw, Phys. Rev. A **75**, 022513 (2007).
[12] N. T. Maitra, R. van Leeuwen, and K. Burke, Phys. Rev. A **78**, 056501 (2008).
[13] J. Schirmer and A. Dreuw, Phys. Rev. A **78**, 056502 (2008).
[14] J. P. Perdew, K. Burke, and M. Ernzerhof, Phys. Rev. Lett. **77**, 3865 (1996).
[15] C. Adamo and V. Barone, J. Chem. Phys. **110**, 6158 (1999).
[16] J. P. Perdew, M. Ernzerhof, and K. Burke, J. Chem. Phys. **105**, 9982 (1996).
[17] D. Jacquemin, E. A. Perpète, G. E. Scuseria, I. Ciofini, and C. Adamo, J. Chem. Theory Comput. **4**, 123 (2008).
[18] M. Schreiber, V. Buß, and M. P. Fülscher, Phys. Chem. Chem. Phys. **3**, 3906 (2001).
[19] J. Fabian, Theor. Chem. Acc. **106**, 199 (2001).
[20] C.-P. Hsu, S. Hirata, and M. Head-Gordon, J. Phys. Chem. A **105**, 451 (2001).
[21] S. Grimme and M. Parac, ChemPhysChem **4**, 292 (2003).
[22] M. Parac and S. Grimme, Chem. Phys. **292**, 11 (2003).
[23] J. H. Starcke, M. Wormit, J. Schirmer, and A. Dreuw, Chem. Phys. **329**, 39 (2006).
[24] J. Fabian, Dyes Pigm. **84**, 36 (2010).
[25] S. Di Tommaso, D. Bousquet, D. Moulin, F. Baltenneck, P. Riva, H. David, A. Fadli, J. Gomar, I. Ciofini, and C. Adamo, J. Comput. Chem. **38**, 998 (2017).
[26] B. Calitree, D. J. Donnelly, J. J. Holt, M. K. Gannon, C. L. Nygren, D. K. Sukumaran, J. Autschbach, and M. R. Detty, Organometallics **26**, 6248 (2007).
[27] T. Lazarides, T. M. McCormick, K. C. Wilson, S. Lee, D. W. McCamant, and R. Eisenberg, J. Am. Chem. Soc. **133**, 350 (2011).
[28] S. Grimme and F. Neese, J. Chem. Phys. **127**, 154116 (2007).
[29] A. E. Masunov, Int. J. Quantum Chem. **110**, 3095 (2010).
[30] C. M. Marian and N. Gilka, J. Chem. Theory Comput. **4**, 1501 (2008).
[31] B. Champagne, M. Guillaume, and F. Zutterman, Chem. Phys. Lett. **425**, 105 (2006).
[32] B. Le Guennic and D. Jacquemin, Acc. Chem. Res. **48**, 530 (2015).
[33] B. Moore and J. Autschbach, J. Chem. Theory Comput. **9**, 4991 (2013).
[34] H. Zhekova, M. Krykunov, J. Autschbach, and T. Ziegler, J. Chem. Theory Comput. **10**, 3299 (2014).
[35] M. Petersilka, U. J. Gossmann, and E. K. U. Gross, Phys. Rev. Lett. **76**, 1212 (1996).
[36] M. E. Casida, "Time-dependent density functional response theory for molecules," in *Recent Advances in Density Functional Methods*, edited by P. Chong (World Scientific, Singapore, 1995), pp. 155–192.
[37] S. R. Yost and T. Van Voorhis, J. Phys. Chem. C **117**, 5617 (2013).
[38] A. R. Kshirsagar, G. D'Avino, X. Blase, J. Li, and R. Poloni, J. Chem. Theory Comput. **16**, 2021 (2020).
[39] O. V. Ovchinnikov, A. V. Evtukhova, T. S. Kondratenko, M. S. Smirnov, V. Y. Khokhlov, and O. V. Erina, Vib. Spectrosc. **86**, 181 (2016).
[40] A. J. Cohen, P. Mori-Sánchez, and W. Yang, Science **321**, 792 (2008).
[41] J. J. Eriksen, S. P. A. Sauer, K. V. Mikkelsen, O. Christiansen, H. J. A. Jensen, and J. Kongsted, Mol. Phys. **111**, 1235 (2013).
[42] A. Eilmes, Theor. Chem. Acc. **133**, 1538 (2014).
[43] T. B. de Queiroz and S. Kümmel, J. Chem. Phys. **141**, 084303 (2014).
[44] D. J. Tozer, J. Chem. Phys. **119**, 12697 (2003).
[45] A. Dreuw and M. Head-Gordon, J. Am. Chem. Soc. **126**, 4007 (2004).
[46] T. Stein, L. Kronik, and R. Baer, J. Am. Chem. Soc. **131**, 2818 (2009).
[47] T. Yanai, D. P. Tew, and N. C. Handy, Chem. Phys. Lett. **393**, 51 (2004).
[48] Y. Tawada, T. Tsuneda, S. Yanagisawa, T. Yanai, and K. Hirao, J. Chem. Phys. **120**, 8425 (2004).
[49] T. M. Henderson, B. G. Janesko, and G. E. Scuseria, J. Chem. Phys. **128**, 194105 (2008).
[50] S. Kümmel, Adv. Energy Mater. **7**, 1700440 (2017).
[51] J.-D. Chai and M. Head-Gordon, J. Chem. Phys. **128**, 084106 (2008).
[52] O. A. Vydrov and G. E. Scuseria, J. Chem. Phys. **125**, 234109 (2006).
[53] O. A. Vydrov, J. Heyd, A. V. Krukau, and G. E. Scuseria, J. Chem. Phys. **125**, 074106 (2006).
[54] R. Baer, E. Livshits, and U. Salzner, Annu. Rev. Phys. Chem. **61**, 85 (2010).
[55] T. B. de Queiroz and S. Kümmel, J. Chem. Phys. **143**, 034101 (2015).
[56] S. Refaely-Abramson, R. Baer, and L. Kronik, Phys. Rev. B **84**, 075144 (2011).
[57] A. Karolewski, T. Stein, R. Baer, and S. Kümmel, J. Chem. Phys. **134**, 151101 (2011).
[58] V. Ziaei and T. Bredow, ChemPhysChem **18**, 579 (2017).
[59] D. Raithel, S. Baderschneider, T. B. de Queiroz, R. Lohwasser, J. Köhler, M. Thelakkat, S. Kümmel, and R. Hildner, Macromolecules **49**, 9553 (2016).
[60] H. Sekino, Y. Maeda, M. Kamiya, and K. Hirao, J. Chem. Phys. **126**, 014107 (2007).
[61] P. Boulanger, D. Jacquemin, I. Duchemin, and X. Blase, J. Chem. Theory Comput. **10**, 1212 (2014).
[62] C. Azarias, I. Duchemin, X. Blase, and D. Jacquemin, J. Chem. Phys. **146**, 034301 (2017).
[63] P. Deglmann, F. Furche, and R. Ahlrichs, Chem. Phys. Lett. **362**, 511 (2002).
[64] P. Deglmann and F. Furche, J. Chem. Phys. **117**, 9535 (2002).
[65] M. L. Sánchez, M. A. Aguilar, and F. J. O. del Valle, J. Comput. Chem. **18**, 313 (1997).
[66] M. L. Sánchez, M. E. Martín, M. Aguilar, and F. Olivares del Valle, J. Comput. Chem. **21**, 705 (2000).
[67] K. Coutinho and S. Canuto, *Advances in Quantum Chemistry* (Elsevier, 1997), Vol. 28, pp. 89–105.
[68] K. Coutinho, H. C. Georg, T. L. Fonseca, V. Ludwig, and S. Canuto, Chem. Phys. Lett. **437**, 148 (2007).
[69] C. M. Breneman and K. B. Wiberg, J. Comput. Chem. **11**, 361 (1990).
[70] V. Ludwig, K. Coutinho, and S. Canuto, Phys. Chem. Chem. Phys. **9**, 4907 (2007).

[71]R. C. Barreto, K. Coutinho, H. C. Georg, and S. Canuto, Phys. Chem. Chem. Phys. **11**, 1388 (2009).
[72]V. Manzoni, M. L. Lyra, R. M. Gester, K. Coutinho, and S. Canuto, Phys. Chem. Chem. Phys. **12**, 14023 (2010).
[73]J. C. Dean, S. Rafiq, D. G. Oblinsky, E. Cassette, C. C. Jumper, and G. D. Scholes, J. Phys. Chem. A **119**, 9098 (2015).
[74]J. J. Nogueira, M. Oppel, and L. González, Angew. Chem., Int. Ed. **54**, 4375 (2015).
[75]D. Jacquemin, I. Duchemin, A. Blondel, and X. Blase, J. Chem. Theory Comput. **13**, 767 (2017).
[76]X. Gui, C. Holzer, and W. Klopper, J. Chem. Theory Comput. **14**, 2127 (2018).
[77]D. Jacquemin, I. Duchemin, and X. Blase, J. Phys. Chem. Lett. **8**, 1524 (2017).
[78]T. Rangel, S. M. Hamed, F. Bruneval, and J. B. Neaton, J. Chem. Phys. **146**, 194108 (2017).
[79]D. Niedzialek, I. Duchemin, T. B. de Queiroz, S. Osella, A. Rao, R. Friend, X. Blase, S. Kümmel, and D. Beljonne, Adv. Funct. Mater. **25**, 1972 (2015).
[80]I. Schelter, J. M. Foerster, A. T. Gardiner, A. W. Roszak, R. J. Cogdell, G. M. Ullmann, T. B. de Queiroz, and S. Kümmel, J. Chem. Phys. **151**, 134114 (2019).
[81]L. Kronik and S. Kümmel, Adv. Mater. **30**, 1706560 (2018).
[82]A. G. Gilani, M. Salmanpour, and T. Ghorbanpour, J. Mol. Liq. **179**, 118 (2013).
[83]E. Tapavicza, F. Furche, and D. Sundholm, J. Chem. Theory Comput. **12**, 5058 (2016).
[84]E. Tapavicza, J. Phys. Chem. Lett. **10**, 6003 (2019).
[85]C. Cisneros, T. Thompson, N. Baluyot, A. C. Smith, and E. Tapavicza, Phys. Chem. Chem. Phys. **19**, 5763 (2017).
[86]E. Tapavicza, T. Thompson, K. Redd, and D. Kim, Phys. Chem. Chem. Phys. **20**, 24807 (2018).